Chinese Journal of Catalysis 52 (2023) 271–279

available at www.sciencedirect.com

ScienceDirect

journal homepage: www.sciencedirect.com/journal/chinese-journal-of-catalysis

Article

Electronic effects of redox-active ligands on ruthenium-catalyzed water oxidation

Jing Shi [a,b], Yu-Hua Guo [b], Fei Xie [b], Ming-Tian Zhang [b,*], Hong-Tao Zhang [b,*]

[a] *Jiangsu Key Laboratory of Advanced Catalytic Materials & Technology, School of Petrochemical Engineering, Changzhou University, Changzhou 213164, Jiangsu, China*

[b] *Center of Basic Molecular Science (CBMS), Department of Chemistry, Tsinghua University, Beijing 100084, China*

ARTICLE INFO

Article history:
Received 12 June 2023
Accepted 28 July 2023
Available online 25 September 2023

Keywords:
Artificial photosynthesis
Water oxidation
Redox-active ligand
Ru^{IV}=O intermediate
Substituent effect

ABSTRACT

The process of water oxidation presents a significant challenge in the development of artificial photosynthetic systems. This complexity arises from the necessity of charge accumulation, involving four electrons and four protons, and O–O bond formation. The strategy of using redox-active ligands in conjunction with metals is recognized as an effective approach for managing this charge accumulation process, attracting considerable attention. However, the detailed mechanisms by which the electronic effect of the redox-active ligands affect the reactivity of the catalytic centers remain ambiguous. In this study, the electronic effect of a series of mononuclear Ru complexes furnished with redox-active ligands ($[(L_R^{N5-})Ru^{III}\text{-}OH]^+$, R = OMe, **3a**; Me, **3b**; H, **3c**; F, **3d**; CF_3, **3e**) was examined on water oxidation. A correlation was observed between redox potentials and substituent constants (σ_{para}), indicating that different successive redox pairs are influenced by electron effects of varying intensities. Particularly, the ligand-centered oxidation (E $\{[(L^{N5-})^{+\bullet}Ru^{IV}=O]^{2+}/[(L^{N5-})Ru^{IV}=O]^{+}\}$) shows a greater dependence than the metal-centered PCET oxidations, $E(Ru^{III}\text{-}OH/Ru^{II}\text{-}OH_2)$ and $E(Ru^{IV}=O/Ru^{III}\text{-}OH)$. The critical intermediate, $[(L^{N5-})^{+\bullet}Ru^{IV}=O]^{2+}$, formed through ligand-centered oxidation, triggers O–O bond formation *via* its reaction with water. The rate constants of this crucial step can be effectively modulated by the substituents of the ligand. This study provides intricate insights into the role of the redox-active ligand in regulating the water oxidation process and further substantiates the effectiveness of the synergistic interaction of redox ligands and metals in controlling the multi-electron catalytic process.

1. Introduction

Water oxidation, which involves the conversion of two molecules of water into oxygen, four protons, and four electrons ($2H_2O \rightarrow O_2 + 4H^+ + 4e^-$), is a vital half-reaction. This process presents significant challenges for artificial photosystems due to the necessity of successive $4H^+/4e^-$ transfers, a high thermodynamic potential (1.23 V *vs.* NHE, pH = 0), and the slow formation of O–O bond [1–4]. In nature, these challenges are adeptly managed by the $CaMn_4O_5$ cluster within photosystem II (PSII), which demonstrates efficient catalytic performance [5–7]. Inspired by that, numerous molecular water oxidation catalysts (WOCs) have been developed based on noble metals ruthenium [8–22], iridium [23–28] and earth-abundant metals

* Corresponding author. E-mail: mtzhang@mail.tsinghua.edu.cn (M.-T. Zhang), zhanght18@tsinghua.org.cn (H.-T. Zhang).
This work was supported by the National Natural Science Foundation of China (21933007, 22193011, 22201024), the Natural Science Foundation of Jiangsu Province (BK20220617), the Natural Science Foundation of the Jiangsu Higher Education Institutions of China (21KJB150005), and the China Postdoctoral Science Foundation (2023T160358).
https://doi.org/10.1016/S1872-2067(23)64497-3

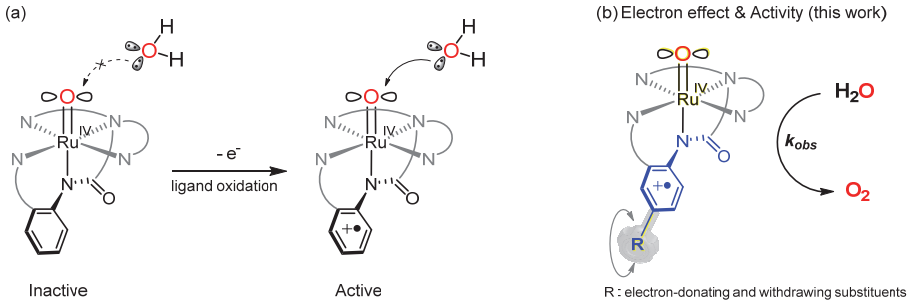

Fig. 1. (a) Redox ligand-assisted water nucleophilic attacked on Ru^{IV}=O in water oxidation catalysis. (b) This study: the core structures of the designed Ru^{IV}=O intermediates with different substituents to explore the relationship between the electron effect and catalytic activity.

manganese [29–32], iron [33–39], cobalt [40–44], nickel [45–47], and copper [48–56], after the first homogeneous WOC (Blue dimer) reported in 1982 [57]. Significant strides have been made in understanding the mechanisms behind catalytic water oxidation, particularly with well-defined molecular catalysts [58–61], and notably with ruthenium systems [62–64]. For instance, a mechanism involving a single-site Ru catalyst [15,65], where water launches a nucleophilic attack on high-valent Ru^{V}=O to form O–O bonds (known as the WNA pathway), was first proposed by Meyer [65] and subsequently corroborated by Lloret-Fillol [66]. However, despite these advancements, the scientific community continues to seek a deeper understanding of the mechanistic details. This includes a focus on how to regulate the reactivity of high-valent Ru=O intermediates.

In a recent study, we discovered that a redox-active ligand assists in charge accumulation through proton-coupled electron transfer (PCET). This process further aids the formation of an O–O bond by moderating the reactivity of the Ru^{IV}=O species toward a water nucleophilic attack (Fig. 1(a)) [67]. However, there remain several unresolved queries regarding the role of the redox-active ligand in catalysis involving multiple electrons and protons. Consequently, we sought to examine the water oxidation mechanisms in detail, specifically for the $[(L_R^{N5-})Ru^{III}\text{-}OH]^+$, catalyst, where ligand oxidation is crucial in instigating O–O bond formation *via* Ru^{IV}=O at a pH of 7.0. By incorporating both electron-donating and electron-withdrawing substituents at the redox-active ligand site (Fig. 1(b)), we can deduce how the ligand's electronic attributes influence the catalyst's activity while preserving a consistent local ligand environment. With this objective, we evaluated a series of structurally similar ruthenium complexes $[(L_H^{N5-})Ru^{III}\text{-}OH]^+$, featuring both electron-donating and electron-withdrawing groups at the para-position of the *N*-phenylacetamide segments (R = OCH_3 (**3a**), CH_3 (**3b**), F (**3d**), or CF_3 (**3e**), Scheme 1) in this study. Electrochemical analyses demonstrated that these added substituents can modulate the redox potential of the complexes through the electronic effect of the ligand. In the consecutive three-step oxidation, the impact of the substituent on the redox potentials progressively intensified, signifying that the ligand center was oxidized in the third step, forming the $[(L^{N5-})^{+\bullet}Ru^{IV}=O]^{2+}$ intermediate. Under catalytic conditions, the overpotentials of these catalyst families significantly diminished with the increasing electron-donating influence of the substituents. The Hammett correlation (ρ = 1.0) between k_{obs} and σ_{para} further demonstrates that O–O bond formation *via* the nucleophilic attack of water on the Ru^{IV}=O unit corresponds to the rate-determining step in the catalytic cycle. These detailed investigations clarify how the redox-active ligand enables easier access to higher redox levels of the metal ion and manages the reactivity of Ru^{IV}=O towards O–O bond formation.

2. Experimental

2.1. Materials

All chemicals used in this study, except ligands **1a–1e** and complexes **2a–2e** and **3a–3e**, were purchased from a commercial company and used without further purification, unless otherwise specified. Deionized water was purified using a Milli-Q ultrapure water purification system.

2.2. Instrumentation

^1H and ^{13}C NMR spectra were recorded on a Bruker Avance 400 spectrometer, ESI-HRMS data were recorded on an LCMS-IT/TOF (Shimadzu, Japan), and X-ray diffraction studies were conducted using an Xcalibur E X-ray single-crystal diffractometer. The data were collected using four-circle kappa diffractometers equipped with CCD detectors. The data were reduced and corrected for absorption [68]. Solution, refinement, and geometrical calculations for all crystal structures were performed using SHELXTL-97, and PLATON SQUEEZE was used to remove the undetermined disordered solvent [69].

All electrochemical data were collected using a CHI-630

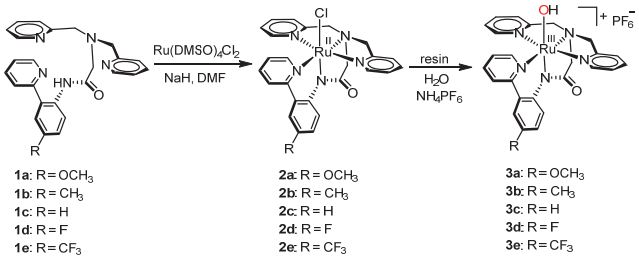

Scheme 1. Synthetic procedure and structures of the ruthenium (III) complexes $[(L_R^{N5-})Ru^{III}\text{-}OH]^+$ (R = OMe, **3a**; Me, **3b**; H, **3c**[67]; F, **3d**; CF_3, **3e**).

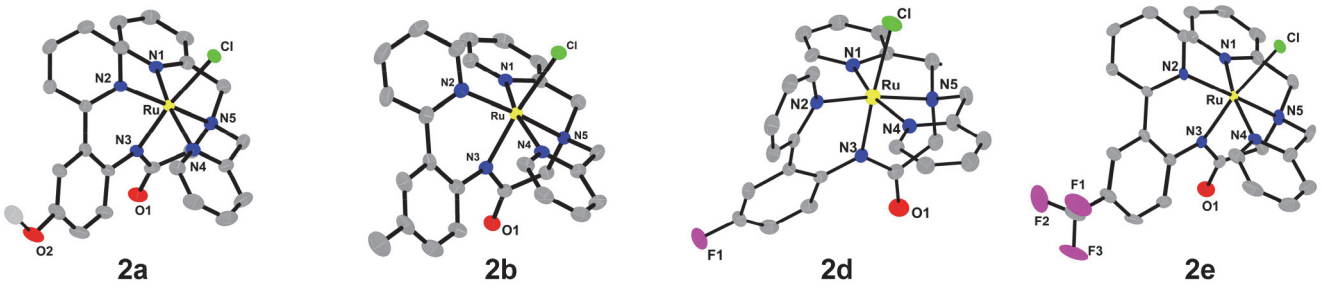

Fig. 2. Crystallographic structures of **2a** (CCDC 1977765), **2b** (CCDC 1977762), **2d** (CCDC 1977769), and **2e** (CCDC 1977767)**.** The thermal ellipsoids are displayed at a 30% probability. Hydrogen atoms and solvents have been omitted for clarity.

electrochemical workstation, and a three-electrode system was applied. Specifically, the working electrode (WE) was a glassy carbon electrode (GC, 0.07 cm^2), counter electrode (CE) was a platinum wire electrode, and reference electrode (RE) was a saturated calomel electrode ($Hg/HgCl_2$, saturated KCl solution) for the aqueous phase or an $AgNO_3/Ag$ electrode for the organic phase. Before electrochemical experiments, GC electrode was required to be polished continuously with 0.3 and 0.05 μm alumina (Al_2O_3). Subsequently, it was washed and cleaned with the deionized water. All potentials used in this study were corrected using a normal hydrogen electrode (NHE, in aqueous solution) or ferrocene ($Fc^{+/0}$ in an organic solvent).

3. Results and discussion

3.1. Synthesis and Characterization

Our previous study showed that the redox-active site of the ligand significantly improved the reactivity of Ru^{IV}=O toward water oxidation [67]. Therefore, the substituents were installed at the para-position of the *N*-phenylacetamide fragment, which not only avoided the steric hindrance effect but also maintained the original coordinated geometry. These redox ligands (**1a**–**1e**) and the corresponding Ru complexes (**2a**–**2e** and **3a**–**3e**) were prepared (Scheme 1; synthetic details are listed in the SI) and characterized *via* ^{1}H NMR (Figs. S9–S16), ^{13}C NMR (Figs. S25–S28), and ESI-HRMS (Figs. S35–S42). The molecular structures of **2a**–**2b** and **2d**–**2e** were further verified using single-crystal X-ray diffraction (Fig. 2). All the structures displayed a typical distorted octahedral geometry around the Ru^{II} center, similar to the reported structure of **2c** [(L_H^{N5-})Ru^{II}-Cl] [67]. These ligands with different substituents, **1a**–**1e,** coordinate with the Ru atom *via* five N atoms, and an extra Cl^- anion is in *trans* position to the amidate N atom. Similar to the synthesis of **3c** [(L_H^{N5-})Ru^{III}-OH]$^+$ [67], hydroxylated **3a**–**3b** and **3d**–**3e** were also prepared using the corresponding chlorides **2a**–**2e** and characterized *via* ESI-HRMS (Figs. S39–S42).

3.2. Redox properties of the prepared ruthenium complexes

To investigate the effect of the substituents on the redox properties of **3a–3e**, cyclic voltammetry (CV) and differential pulse voltammetry (DPV) were conducted in propylene carbonate (PC) using a GC electrode. The potentials were corrected using $Fc^{+/0}$ in propylene carbonate. As shown in Fig. 3(a), all five complexes displayed three successive reversi-

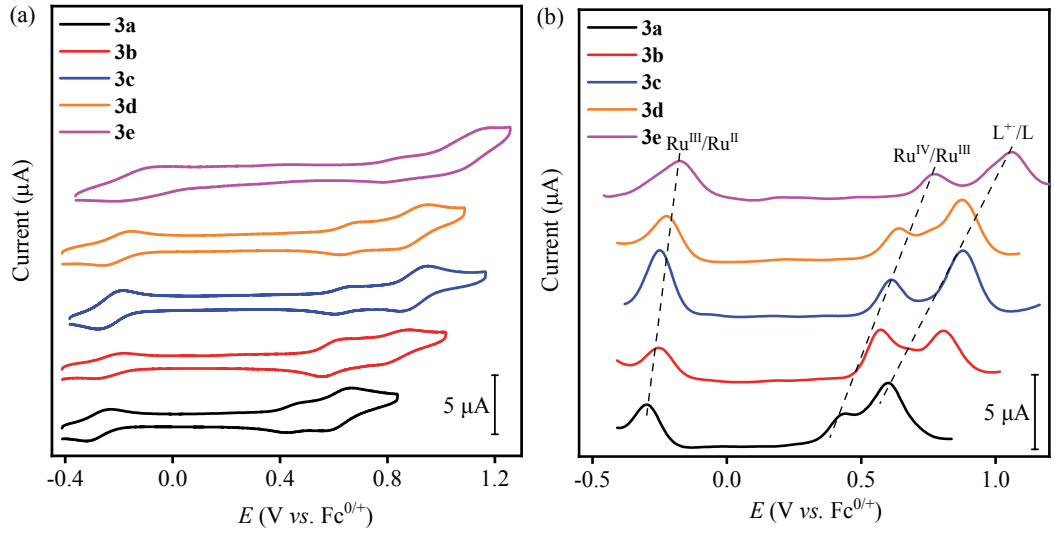

Fig. 3. CVs (a) and DPVs (b) of 1.0 mmol/L **3a–3e.** They were obtained using a glassy carbon (GC) electrode in 0.1 mol/L ^{n}Bu_4NPF_6 propylene carbonate solution.

Table 1
Summary of redox potentials (*vs.* $Fc^{+/0}$) for Ru-based complexes **3a–3e** in propylene carbonate [a].

Complexe	*R*	σ_{para} [b]	$Ru^{III/II}$	$Ru^{IV/III}$	$L^{+\bullet}Ru^{IV}/LR$
3a	OCH_3	–0.27	–0.30	0.44	0.60
3b	CH_3	–0.17	–0.27	0.56	0.80
3c	H	0	–0.23	0.63	0.90
3d	F	0.06	–0.22	0.64	0.88
3e	CF_3	0.54	–0.16	0.78	1.07

[a] All potentials are obtained from the DPV tests in Fig. 3(b). [b] These Hammett substitution constants (σ_{para}) describe the effects of para substitution on benzoic acid, as obtained from ref. [70].

ble/quasi-reversible redox waves. Based on the reported DFT calculations of **3c** $[(L_HN5^-)Ru^{III}\text{-}OH]^+$ [67], the three oxidative processes were assigned to the metal oxidation of $Ru^{III/II}$ and $Ru^{IV/III}$ couples and ligand-centered oxidation (Fig. 3(b)). The corresponding oxidative potentials of this family of Ru complexes are presented in Table 1. As anticipated, the potentials of each redox couple increased as the electron-donating ability decreased. To compare the influence of the electronic properties of the substituents on the three oxidative processes, Hammett-correlated curves between the redox potentials of **3a–3e** and substituent constants (σ_{para}) are plotted and fitted linearly, as shown in Fig. 4. The results showed that the first two (proton-coupled) electron-transfer processes were slightly affected by the substituent groups, with slopes of 0.17 and 0.38, but the ligand-centered oxidation step was significantly affected with an observed slope of 0.50. The variations in the slopes were attributed to the following: for the first two processes, the metal center lies far away from the substituent groups, resulting in less electron density change on the metal center; thus, the first two oxidation processes show relatively small slopes; however, the third oxidation process occurs at the ligand center, and the redox property of the ligand center can be easily regulated by the attached substituent groups. Hence, the third oxidation displays a large slope. These experimental results reveal that the ligand can undertake a partial charge and avoid excessive charge accumulation at the metal site. Additionally, upon gradual addition of water to the PC solutions of **3a–3b** and **3d–3e**,

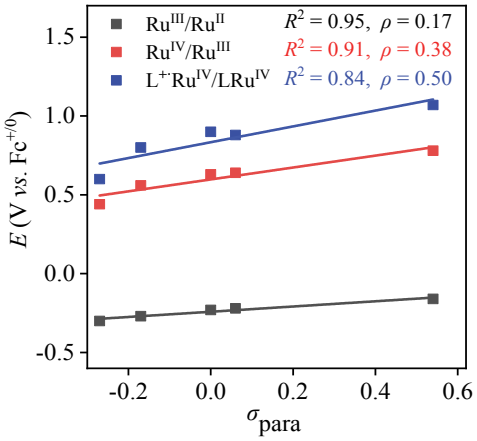

Fig. 4. Hammett correlation between redox potentials and substituent constants σ_{para} for Ru catalysts **3a–3e** in PC.

the first two waves remained reversible or quasi-reversible, but the ligand-centered oxidation became irreversible, and the anodic current increased (Figs. S43 and S44). These electrochemical behaviors were consistent with those of **3c**, indicating an electrocatalytic water oxidation event.

3.3. Electrocatalytic performance of ruthenium complexes for water oxidation.

To examine the influence of the introduced substituents on the catalytic water oxidation, complexes **3a–3e** were also investigated *via* electrochemical methods in aqueous phosphate buffer solutions (PBS, 0.1 mol/L, pH=7.0) at room temperature (Fig. 5). All potentials reported in the aqueous solution were compared to those of the normal hydrogen electrode (NHE). Considering **3c** as the reference catalyst [67], the other Ru complexes also displayed three oxidative events in CVs (Fig. 5), which were assigned to $Ru^{III/II}$, $Ru^{IV/III}$, and $L^{+\bullet}/L$. In the third oxidative wave, all Ru complexes exhibited rapid incremental currents, indicating catalytic processes. Moreover, the CVs of all complexes were documented at different scan rates, and the resulting normalized catalytic currents of the third wave were strongly dependent on the scan rate (Figs. S45–S48), which is consistent with the catalytic water oxidation process. Notably, the catalytic overpotentials of the Ru complexes **3a–3e** were strongly affected by the nature of the introduced substituents (Fig. 6(a)); stronger electron-donating groups led to larger negative shifts in the onset potentials. However, the electron-withdrawing groups were reversed (Table 2). This trend was expected based on the electronic effect of the substituents, as electron-donating groups are more readily able to allow the

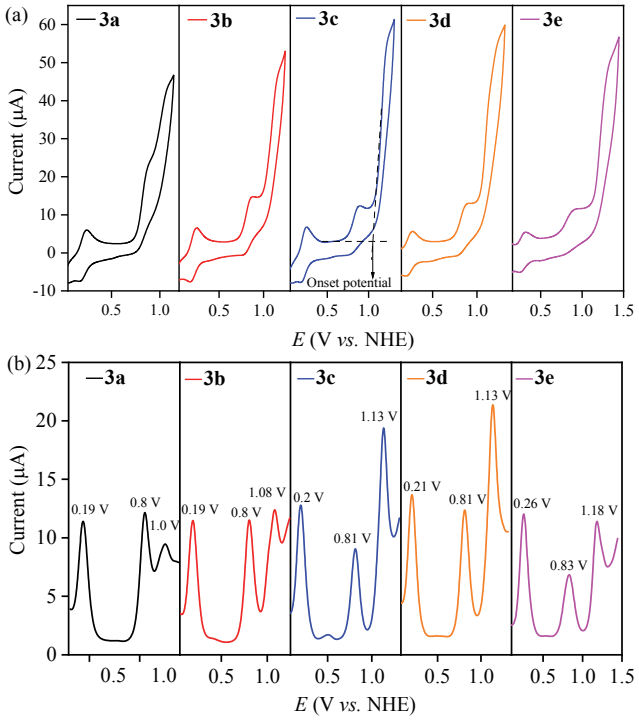

Fig. 5. CVs at 100 mV/s scan rate (a) and DPVs (b) of 1.0 mmol/L **3a–3e** obtained *via* GC electrode in 0.1 mol/L PBS (pH = 7.0).

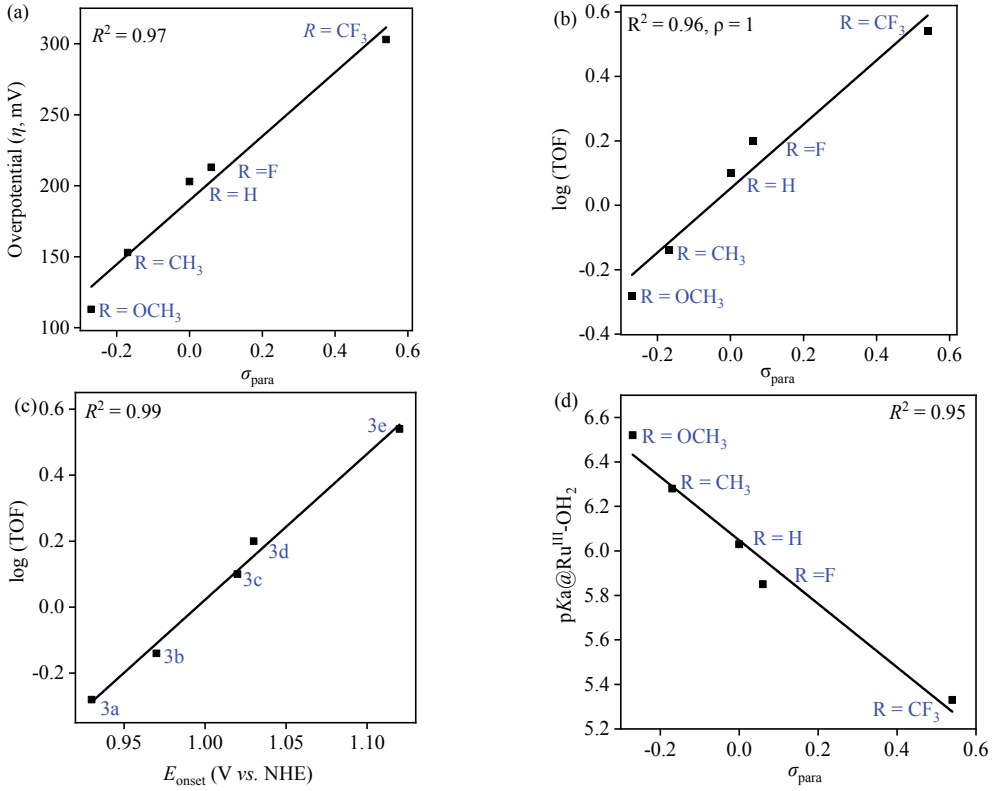

Fig. 6. Correlation between overpotential and σ_{para} (a), correlation between k_{obs} and σ_{para} (b), correlation between k_{obs} and onset potential (c), and correlation between pK_a of $[(L_R^{N5-})Ru^{III}\text{-}OH_2]^{2+}$ and σ_{para} (d) for Ru catalysts **3a–3e** in 0.1 mol/L PBS (pH = 7.0).

oxidation of the ligand center.

3.4. Catalytic kinetics and mechanistic analysis of ruthenium catalysts

According to the above discussion, complexes **3a–3e** can act as catalysts to electrocatalyze water oxidation. However, there are some differences in the onset potentials and k_{obs} (Table 2). To better understand the electrocatalytic behavior of the catalysts, we further investigated the redox properties of **3a–3e** at different pH values and performed a kinetic analysis of the catalytic process.

3.4.1. Kinetics analysis.

Figs. S49–S52 show that the peak currents of the diffusion-controlled and catalytic processes are linearly dependent on the bulk concentrations of the catalyst, **3a–3b** and **3d–3e**. Thus, the reversible process obeys the Randles-Svecik equation in Eq. (1), and the peak current of the catalytic process can be expressed using Eq. (2) [71]. In these equations, F denotes the Faraday constant, A denotes the electrode surface area, i_d denotes the peak current of the diffusion-controlled wave, and i_{cat} denotes the peak current of the catalytic wave. Furthermore, the bulk concentration of the catalyst is denoted by [cat.], while D_{cat} denotes the diffusion coefficient of the catalyst. Here, n_{cat} = 4 signifies the electrochemical stoichiometry for water oxidation.

$$i_d = 0.496 n_d F A[\text{Cat.}](n_d F v D_{cat}/RT)^{0.5} \quad (1)$$

$$i_{cat} = n_{cat} F A[\text{Cat.}](k_{obs} D_{cat})^{0.5} \quad (2)$$

Based on the plot of i_{cat}/i_d versus $v^{-0.5}$ in the same ranges (Figs. S45–S48), the observed rate constant for water oxidation catalysis, k_{obs}, is determined as 0.52, 0.72, 1.26 [67], 1.60, and 3.47 s^{-1} for **3a–3e**, respectively. Furthermore, a linear relationship between introduced substituent constants (σ_{para}) and the k_{obs} can be established (Fig. 6(b)). This linear Hammett plot indicates that the substituents fine-tune the electronic parameters of the catalytic center, and the catalytic rate-determining step remains unchanged. The activities of complexes **3a–3e** increased with increasing substituent constants, indicating that electron-withdrawing substituents accelerate the rate of water oxidation. This is due to the fact that the electron-withdrawing group decreases the electron density of the metal center, which enhances the oxidation of $[(L_R^{N5-})^{+\bullet}Ru^{IV}=O]^{2+}$ species. The Hammett reaction constant slope result, ρ = 1.00, indicates a

Table 2
Summary of electrochemical data, determined pK_a values, and catalytic parameters for Ru catalysts **3a–3e** in 0.1 mol/L PBS (pH = 7.0).

Complexe	R	E_{onset} (V *vs.* NHE)	Overpotential (mV)[b]	k_{obs} (s^{-1})	pK_a
3a	OCH_3	0.93[a]	113	0.52	6.52
3b	CH_3	0.97	153	0.72	6.28
3c	H	1.02	203	1.26	6.03
3d	F	1.03	213	1.60	5.85
3e	CF_3	1.12	303	3.47	5.33

[a] The E_{onset} of **3a** was estimated from CV because of interference from the second oxidation wave. [b] The overpotentials were determined by subtracting the theoretical potential at pH = 7.0 (0.817 V *vs.* NHE) from E_{onset}.

significant reduction in positive charge during the rate-determining step. Furthermore, the activities of complexes **3a–3e** also escalated with increasing onset potentials (Fig. 6(c)) due to the more favorable thermodynamic driving force at higher potentials. Reducing the onset potential necessitates the presence of electron-donating groups, while increasing the catalytic activity calls for electron-withdrawing groups. Consequently, modifications to molecular catalysts often result in a trade-off between k_{obs} and the effective overpotential (η_{eff}) for initiating catalysis.

3.4.2. *Protons and electrons transfer in water oxidation catalysis.*

In line with the Nernst equation, Pourbaix diagrams (Figs. S53–S56) for catalysts **3a**–**3b** and **3d**–**3e** can be generated DPV experiments conducted under varying pH conditions (Figs. S57–S60). These diagrams display electrochemical oxidative behaviors similar to those of catalyst **3c** in the *E*-pH diagram [67]. The first reversible wave transitioned from being pH-independent (Eq. (3)) to pH-dependent for catalysts **3a**–**3e**, respectively, demonstrating slopes of approximately 57–60 mV/pH (Eq. (4)) within the pH range of 5.3–6.5, as indicated in Eqs. (3) and (4).

$$[(L_R^{N5-})Ru^{II}\text{-}OH_2]^+ - e^- \rightarrow [(L_R^{N5-})Ru^{III}\text{-}OH_2]^{2+} \quad (3)$$

$$[(L_R^{N5-})Ru^{II}\text{-}OH_2]^+ - e^- - H^+ \rightarrow [(L_R^{N5-})Ru^{III}\text{-}OH]^+ \quad (4)$$

The second quasi-reversible waves are strongly pH-dependent with slopes of 100–130 mV/pH (4 < pH < 6, Eq. (5)) and 47–55 mV/pH (pH > 6, Eq. (6)), which conform to proton-coupled electron-transferred oxidative processes.

$$[(L_R^{N5-})Ru^{III}\text{-}OH_2]^{2+} - e^- - 2H^+ \rightarrow [(L_R^{N5-})Ru^{IV}{=}O]^+ \quad (5)$$

$$[(L_R^{N5-})Ru^{III}\text{-}OH]^+ - e^- - H^+ \rightarrow [(L_R^{N5-})Ru^{IV}{=}O]^+ \quad (6)$$

The third oxidative steps are pH-independent process (Eq. (7)), indicating that the generated $[(L_R^{N5-})Ru^{IV}{=}O)]^+$ can be further oxidized *via* one-electron process to provide $[(L_R^{N5-})^{+\bullet}Ru^{IV}{=}O]^{2+}$ intermediate with oxidized ligand. Furthermore, DFT calculations confirmed that the *N*-phenylacetamide moiety of the $[(L_R^{N5-})^{+\bullet}Ru^{IV}{=}O]^{2+}$ intermediates exhibited obvious spin populations and antiferromagnetic couples with the metal center (Table S1).

$$[(L_R^{N5-})Ru^{IV}{=}O]^+ - e^- \rightarrow [(L_R^{N5-})^{+\bullet}Ru^{IV}{=}O]^{2+} \quad (7)$$

Additionally, the pK_a data for $[(L_R^{N5-})Ru^{III}\text{-}OH_2]^{2+}$ were extracted from the respective Pourbaix diagrams as follows: 6.52 for **3a**, 6.28 for **3b**, 6.03 for **3c** [67], 5.85 for **3d**, 5.33 for **3e** (Table 2), which exhibited a linear change with the substituent constant (Fig. 6(d)). Stronger electron-donating substituents efficiently increased the electron density at the Ru-OH_2 moiety in the conjugate acid of **3a–3e**, thus increasing pK_a. Conversely, a reverse trend was observed for electron-withdrawing groups.

3.4.3. *Catalytic mechanism analysis of O–O bond formation.*

According to the above discussion, the catalytic peak current for water oxidation, i_{cat}, varies linearly with the catalyst concentration (Figs. S49–S52), which is consistent with single-site ruthenium catalysis. CV experiments on water oxidation were also performed in D_2O (pD 7.4) phosphate buffer (Figs. S61–S64). Analysis of these data revealed that the kinetic isotope effects (KIE = $i_{cat,\ H2O}{}^2/i_{cat,\ D2O}{}^2 = k_{H2O}/k_{D2O}$) of catalysts **3a–3b** and **3d–3e** were 1.40, 1.30, 1.54, and 1.27, respectively. This remarkable KIE was attributed to atom-proton transfer (APT) in the catalytic rate-determining step [72]. Additionally, the electrochemical behavior of the ruthenium catalysts at different buffer concentrations was investigated with a controlled ionic strength of I = 0.462 mol/L in PBS (Figs. S65–S68). The dependence of $(i_{cat}/i_d)^2$ on the phosphate concentration (0–0.2 mol/L) demonstrates that the buffer anion, as a proton acceptor, can contribute to water oxidation [72]. These results are consistent with those of reference catalyst **3c** [67] and fit the WNA pathway. The KIE, buffer effect and linear Hammett correlation collectively revealed that the active $[(L_R^{N5-})^{+\bullet}Ru^{IV}{=}O]^{2+}$ intermediate underwent nucleophilic attack by water molecules to form O–O bonds with the assistance of a base (Eq. (8) and Fig. 7(a)). This is the rate-determining step in the entire cycle. The atomic dipole corrected Hirshfeld atomic charge (ADCH) analysis exhibited that the O atom of $Ru^{IV}{=}O$ unit in the $[(L_R^{N5-})^{+\bullet}Ru^{IV}{=}O]^{2+}$ with electron-withdrawing substituents held less negative charge, while the Ru atom exhibited more positive charge (Table S2). This implies that the electron-withdrawing substituent can improve the reactivity of the

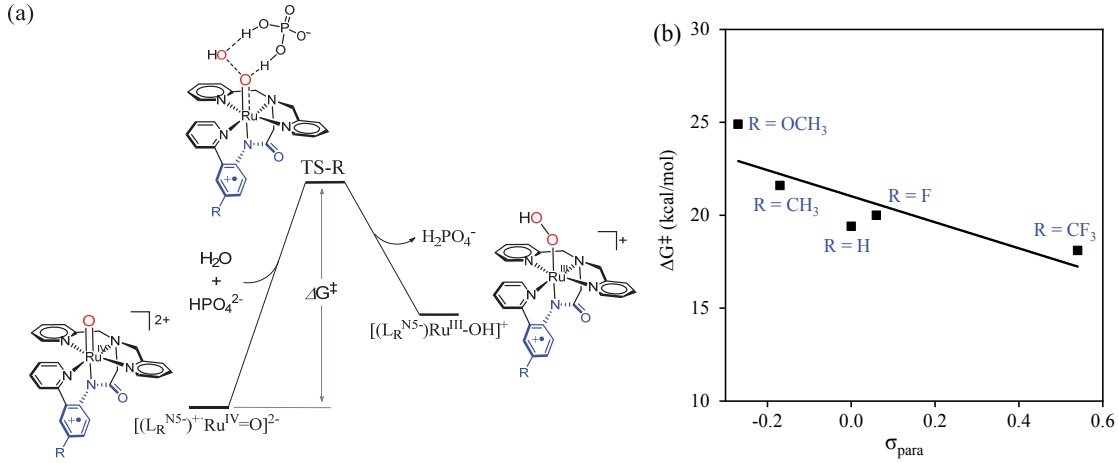

Fig. 7. (a) Energy barrier diagram of the O–O bond forming step *via* H_2O nucleophilic attacking $[(L_R^{N5-})^{+\bullet}Ru^{IV}{=}O]^{2+}$ intermediate. (b) Correlation between the activation Gibbs free energies ($\Delta G^{\ddagger}$) and σ_{para}.

Ru^{IV}=O with water molecule. The energy barriers of this chemical process were evaluated *via* DFT calculations, which revealed that the barriers decreased as the electron-withdrawing ability of the substituents increased (Fig. 7(b)).

$$[(L_R^{N5-})^{+\bullet}Ru^{IV}=O]^{2+} + H_2O + Base^{2-} \rightarrow [(L_R^{N5-})Ru^{III}\text{-}OOH]^{+} + H_2PO_4 \quad (8)$$

In the complex process of water oxidation catalysis, which involves multiple proton/electron transfers, research on a family of mononuclear ruthenium complexes with various substituents has offered deeper insight into the catalytic mechanism and regulation of activity. In this cycle, $[(L_R^{N5-})Ru^{II}\text{-}OH_2]^{+}$ is readily oxidized to $[(L_R^{N5-})Ru^{III}\text{-}OH]^{+}$ at a low potential through the PCET process, with electronic regulation being relatively insignificant due to the smaller thermodynamic driving force required. Next, $[(L_R^{N5-})Ru^{III}\text{-}OH]^{+}$ undergoes further oxidation *via* the same process to form $[(L_R^{N5-})Ru^{IV}=O]^{+}$. This step is only marginally influenced by electronic regulation because the electron density at the metal center is reduced in the preceding step. Electronic regulation becomes critical during ligand oxidation. Here, electron-donating groups ease electron departure from the redox-active site of the ligand, generating $[(L_R^{N5-})^{+\bullet}Ru^{IV}=O]^{2+}$ while electron-withdrawing groups exhibit the reverse effect. Subsequently, the highly electron-deficient $[(L_R^{N5-})^{+\bullet}Ru^{IV}=O]^{2+}$ intermediate is attacked by water, resulting in O–O bond formation. This process is expedited as the electron density at the metal center decreases. Hammett linear analysis reveals that the O–O bond formation pathway is the rate-determining step in the cycle. Following this, $[(L_R^{N5-})Ru^{III}\text{-}OOH]^{+}$ is formed, accompanied by an inner-sphere two-electron transfer from the metal and ligand centers. After a rapid PCET oxidation, dioxygen is released *via* the reductive elimination of the peroxo species, allowing the catalysts to return to their initial state.

4. Conclusions

In this study, a family of mononuclear ruthenium complexes, **3a**–**3d** with substituted redox-active ligands, were prepared for water oxidation catalysis. Electrochemical studies showed that the substituents installed at the para position of the *N*-phenylacetamide moiety had a strong linear correlation with the redox potential and catalytic activity of the complexes. With an increase in the valence of the ruthenium complexes, a more obvious substituent effect suggests that the oxidative center gradually changes from metal to ligand, and $[(L^{N5-})^{+\bullet}Ru^{IV}=O]^{2+}$ species with oxidized ligands finally form. This further supports the idea that redox-active ligands participate in the charge accumulation. In catalysis, the substituent can also linearly regulate the catalytic overpotentials and turnover frequencies in the range of 113–303 mV and 0.5–3.5 s^{-1}, respectively. When the electron-donating ability of the substituents is enhanced, the overpotential of the catalyst is effectively reduced; however, the catalytic activity also decreases. Furthermore, *E*-pH dependence, KIE, buffer effect, and Hammett linear correlation revealed that the O–O bond is formed by the nucleophilic attack of water on Ru^{IV}=O, which is the rate-determining step of the entire cycle. This study provides important insights into the rational design and mechanistic study of lower-valent metal-oxo, such as Ru^{IV}=O, catalyzed by water oxidation.

Conflicts of interest

There are no conflicts to declare.

Electronic supporting information

Supporting information is available in the online version of this article.

References

[1] M. D. Kärkäs, O. Verho, E. V. Johnston, B. Åkermark, *Chem. Rev.*, **2014**, 114, 11863–12001.
[2] B. Zhang, L. Sun, *Chem. Soc. Rev.*, **2019**, 48, 2216–2264.
[3] Q.-F. Chen, Y.-H. Guo, Y.-H. Yu, M.-T. Zhang, *Coord. Chem. Rev.*, **2021**, 448, 214164.
[4] X.-P. Zhang, H.-Y. Wang, H. Zheng, W. Zhang, R. Cao, *Chin. J. Catal.*, **2021**, 42, 1253–1268.

Graphical Abstract

Chin. J. Catal., 2023, 52: 271–279 doi: 10.1016/S1872-2067(23)64497-3

Electronic effects of redox-active ligands on ruthenium-catalyzed water oxidation

Jing Shi, Yu-Hua Guo, Fei Xie, Ming-Tian Zhang *, Hong-Tao Zhang *
Changzhou University; Tsinghua University

Studies investigating electronic effects have confirmed that the WNA-type O–O bond formation can be initiated by lower-valent Ru^{IV}=O centers with the aid of redox-active units. This method presents an effective strategy for reducing the catalytic overpotential.

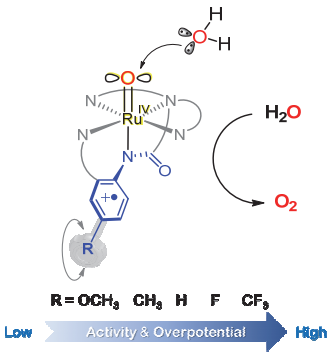

[5] A. Zouni, H. T. Witt, J. Kern, P. Fromme, N. Krauss, W. Saenger, P. Orth, *Nature*, **2001**, 409, 739–743.
[6] N. Kamiya, J.-R. Shen, *Proc. Natl. Acad. Sci. U. S. A.*, **2003**, 100, 98–103.
[7] Y. Umena, K. Kawakami, J.-R. Shen, N. Kamiya, *Nature*, **2011**, 473, 55–60.
[8] J. J. Concepcion, J. W. Jurss, M. K. Brennaman, P. G. Hoertz, A. O. T. Patrocinio, N. Y. Murakami Iha, J. L. Templeton, T. J. Meyer, *Acc. Chem. Res.*, **2009**, 42, 1954–1965.
[9] R. Matheu, M. Z. Ertem, C. Gimbert-Surinach, X. Sala, A. Llobet, *Chem. Rev.*, **2019**, 119, 3453–3471.
[10] S. Romain, L. Vigara, A. Llobet, *Acc. Chem. Res.*, **2009**, 42, 1944–1953.
[11] L. Duan, L. Wang, F. Li, F. Li, L. Sun, *Acc. Chem. Res.*, **2015**, 48, 2084–2096.
[12] L. Duan, F. Bozoglian, S. Mandal, B. Stewart, T. Privalov, A. Llobet, L. Sun, *Nat. Chem.*, **2012**, 4, 418–423.
[13] H. N. Kagalwala, L. Tong, R. Zong, L. Kohler, M. S. Ahlquist, T. Fan, K. J. Gagnon, R. P. Thummel, *ACS Catal.*, **2017**, 7, 2607–2615.
[14] L. Tong, R. P. Thummel, *Chem. Sci.*, **2016**, 7, 6591–6603.
[15] R. Zong, R. P. Thummel, *J. Am. Chem. Soc.*, **2005**, 127, 12802–12803.
[16] T. Wada, K. Tsuge, K. Tanaka, *Inorg. Chem.*, **2001**, 40, 329–337.
[17] J. T. Muckerman, D. E. Polyansky, T. Wada, K. Tanaka, E. Fujita, *Inorg. Chem.*, **2008**, 47, 1787–1802.
[18] Y. Tsubonouchi, S. Lin, A. R. Parent, G. W. Brudvig, K. Sakai, *Chem. Commun.*, **2016**, 52, 8018–8021.
[19] C. Casadevall, Z. Codola, M. Costas, J. Lloret-Fillol, *Chem. Eur. J.*, **2016**, 22, 10111–10126.
[20] Y. Pushkar, D. Moonshiram, V. Purohit, L. Yan, I. Alperovich, *J. Am. Chem. Soc.*, **2014**, 136, 11938–11945.
[21] Y. Xie, D. W. Shaffer, A. Lewandowska-Andralojc, D. J. Szalda, J. J. Concepcion, *Angew. Chem. Int. Ed.*, **2016**, 55, 8067–8071.
[22] M. D. Kärkäs, T. Åkermark, H. Chen, J. Sun, B. Åkermark, *Angew. Chem. Int. Ed.*, **2013**, 52, 4189–4193.
[23] N. D. McDaniel, F. J. Coughlin, L. L. Tinker, S. Bernhard, *J. Am. Chem. Soc.*, **2008**, 130, 210–217.
[24] J. F. Hull, D. Balcells, J. D. Blakemore, C. D. Incarvito, O. Eisenstein, G. W. Brudvig, R. H. Crabtree, *J. Am. Chem. Soc.*, **2009**, 131, 8730–8731.
[25] R. Lalrempuia, N. D. McDaniel, H. Müller-Bunz, S. Bernhard, M. Albrecht, *Angew. Chem. Int. Ed.*, **2010**, 49, 9765–9768.
[26] A. Lewandowska-Andralojc, D. E. Polyansky, C. H. Wang, W. H. Wang, Y. Himeda, E. Fujita, *Phys. Chem. Chem. Phys.*, **2014**, 16, 11976–11987.
[27] J. M. Thomsen, D. L. Huang, R. H. Crabtree, G. W. Brudvig, *Dalton Trans.*, **2015**, 44, 12452–12472.
[28] J. A. Woods, R. Lalrempuia, A. Petronilho, N. D. McDaniel, H. Müller-Bunz, M. Albrecht, S. Bernhard, *Energy Environ. Sci.*, **2014**, 7, 2316–2328.
[29] J. S. Kanady, E. Y. Tsui, M. W. Day, T. Agapie, *Science*, **2011**, 333, 733–736.
[30] C. Zhang, C. Chen, H. Dong, J.-R. Shen, H. Dau, J. Zhao, *Science*, **2015**, 348, 690–693.
[31] G. Maayan, N. Gluz, G. Christou, *Nat. Catal.*, **2018**, 1, 48–54.
[32] S. J. Yang, L. S. Qin, W. Zhang, R. Cao, *Chin. J. Struct. Chem.*, **2022**, 41, 2204022–2204033.
[33] W. C. Ellis, N. D. McDaniel, S. Bernhard, T. J. Collins, *J. Am. Chem. Soc.*, **2010**, 132, 10990–10991.
[34] J. L. Fillol, Z. Codola, I. Garcia-Bosch, L. Gomez, J. J. Pla, M. Costas, *Nat. Chem.*, **2011**, 3, 807–813.
[35] M. K. Coggins, M.-T. Zhang, A. K. Vannucci, C. J. Dares, T. J. Meyer, *J. Am. Chem. Soc.*, **2014**, 136, 5531–5534.
[36] S. DAgostini, K. G. Kottrup, C. Casadevall, I. Gamba, V. Dantignana, A. Bucci, M. Costas, J. Lloret-Fillol, D. G. H. Hetterscheid, *ACS Catal.*, **2021**, 11, 2583–2595.
[37] M. Okamura, M. Kondo, R. Kuga, Y. Kurashige, T. Yanai, S. Hayami, V. K. K. Praneeth, M. Yoshida, K. Yoneda, S. Kawata, S. Masaoka, *Nature*, **2016**, 530, 465–468.
[38] H.-T. Zhang, X.-J. Su, F. Xie, R.-Z. Liao, M.-T. Zhang, *Angew. Chem. Int. Ed.*, **2021**, 60, 12467–12474.
[39] H.-T. Zhang, Y.-H. Guo, Y. Xiao, H.-Y. Du, M.-T. Zhang, *Angew. Chem. Int. Ed.*, **2023**, 62, e202218859.
[40] H.-Y. Du, S.-C. Chen, X.-J. Su, L. Jiao, M.-T. Zhang, *J. Am. Chem. Soc.*, **2018**, 140, 1557–1565.
[41] F. Xie, M.-T. Zhang, *J. Energy Chem.*, **2021**, 63, 1–7.
[42] D. den Boer, Q. Siberie, M. A. Siegler, T. H. Ferber, D. C. Moritz, J. P. Hofmann, D. G. H. Hetterscheid, *ACS Catal.*, **2022**, 12, 4597–4607.
[43] Y.-F. Su, W.-Z. Luo, W.-Q. Lin, Y.-B. Su, Z.-J. Li, Y.-J. Yuan, J.-F. Li, G.-H. Chen, Z. Li, Z.-T. Yu, Z. Zou, *Angew. Chem. Int. Ed.*, **2022**, 61, e202201430.
[44] D. J. Wasylenko, C. Ganesamoorthy, J. Borau-Garcia, C. P. Berlinguette, *Chem. Commun.*, **2011**, 47, 4249–4251.
[45] Q.-F. Chen, Y. Xiao, R.-Z. Liao, M.-T. Zhang, *CCS Chem.*, **2023**, 5, 245–256.
[46] M. Zhang, M.-T. Zhang, C. Hou, Z.-F. Ke, T.-B. Lu, *Angew. Chem. Int. Ed.*, **2014**, 53, 13042–13048.
[47] Y. Han, Y. Wu, W. Lai, R. Cao, *Inorg. Chem.*, **2015**, 54, 5604–5613.
[48] G. Ruan, P. Ghosh, N. Fridman, G. Maayan, *J. Am. Chem. Soc.*, **2021**, 143, 10614–10623.
[49] M. Gil-Sepulcre, P. Garrido-Barros, J. Oldengott, I. Funes-Ardoiz, R. Bofill, X. Sala, J. Benet-Buchholz, A. Llobet, *Angew. Chem. Int. Ed.*, **2021**, 60, 18639–18644.
[50] Q.-F. Chen, Z.-Y. Cheng, R.-Z. Liao, M.-T. Zhang, *J. Am. Chem. Soc.*, **2021**, 143, 19761–19768
[51] S. M. Barnett, K. I. Goldberg, J. M. Mayer, *Nat. Chem.*, **2012**, 4, 498–502.
[52] M.-T. Zhang, Z. Chen, P. Kang, T. J. Meyer, *J. Am. Chem. Soc.*, **2013**, 135, 2048–2051.
[53] T. Zhang, C. Wang, S. Liu, J. L. Wang, W. Lin, *J. Am. Chem. Soc.*, **2014**, 136, 273–281.
[54] X.-J. Su, M. Gao, L. Jiao, R.-Z. Liao, P. E. M. Siegbahn, J.-P. Cheng, M.-T. Zhang, *Angew. Chem. Int. Ed.*, **2015**, 54, 4909–4914.
[55] M. K. Coggins, M.-T. Zhang, Z. Chen, N. Song, T. J. Meyer, *Angew. Chem. Int. Ed.*, **2014**, 53, 12226–12230.
[56] Q.-F. Chen, H.-Y. Du, M.-T. Zhang, *Chin. J. Catal.*, **2021**, 42, 1338–1344.
[57] S. W. Gersten, G. J. Samuels, T. J. Meyer, *J. Am. Chem. Soc.*, **1982**, 104, 4029–4030.
[58] Y. Gao, T. Åkermark, J. Liu, L. Sun, B. Åkermark, *J. Am. Chem. Soc.*, **2009**, 131, 8726–8727.
[59] X. Li, X.-P. Zhang, M. Guo, B. Lv, K. Guo, X. Jin, W. Zhang, Y.-M. Lee, S. Fukuzumi, W. Nam, Rui Cao, *J. Am. Chem. Soc.*, **2021**, 143, 14613–14621.
[60] Z. Codola, L. Gomez, S. T. Kleespies, L. Que Jr, M. Costas, J. Lloret-Fillol, *Nat. Commun.*, **2015**, 6, 5865–5873.
[61] X. Zhang, Q.-F. Chen, J. Deng, X. Xu, J. Zhan, H.-Y. Du, Z. Yu, M. Li, M.-T. Zhang, Y. Shao, *J. Am. Chem. Soc.*, **2022**, 144, 17748–17752.
[62] N. Noll, A.-M. Krause, F. Beuerle, F. Würthner, *Nat. Catal.*, **2022**, 5, 867–877.
[63] J. Yi, S. Zhan, L. Chen, Q. Tian, N. Wang, J. Li, W. Xu, B. Zhang, M. S. G. Ahlquist, *J. Am. Chem. Soc.*, **2021**, 143, 2484–2490.
[64] T. Liu, G. Li, N. Shen, L. Wang, B. J. J. Timmer, S. Zhou, B. Zhang, A.

Kravchenko, B. Xu, M. S. G. Ahlquist, L. Sun, *CCS Chem.,* **2022**, 4, 2481–2490.
[65] J. J. Concepcion, J. W. Jurss, J. L. Templeton, T. J. Meyer, *J. Am. Chem. Soc.*, **2008**, 130, 16462–16463.
[66] C. Casadevall, V. Martin-Diaconescu, W. R. Browne, S. Fernandez, F. Franco, N. Cabello, J. Benet-Buchholz, B. Lassalle-Kaiser, J. Llo-ret-Fillol, *Nat. Chem.*, **2021**, 13, 800–804.
[67] J Shi, Y.-H. Guo, F. Xie, Q.-F. Chen, M.-T. Zhang. *Angew. Chem. Int. Ed.*, **2020**, 59, 4000–4008.
[68] R. H. Blessing, R. H. Blessing, *Acta Crystallogr. Sect. A*, **1995**, 51, 33–38.
[69] G. M. Sheldrick, *Acta Crystallogr. Sect. A*, **2008**, 64, 112–122.
[70] C. Hansch, A. Leo, *Substituent Constants for Correlation Analysis in Chemistry and Biology*, Wiley-Interscience, New York, **1979**.
[71] A. J. Bard, L. R. Faulkner, *Electrochemical methods: Fundamentals, Applications*, Wiley, New York, **2001**.
[72] Z. Chen, J. J. Concepcion, X. Hu, W. Yang, P. G. Hoertz, T. J. Meyer, *Proc. Natl. Acad. Sci. U. S. A.*, **2010**, 107, 7225–7229.

氧化还原活性配体的电子效应对钌催化水氧化反应的影响

石　靖[a,b], 郭煜华[b], 谢　飞[b], 章名田[b,*], 张洪涛[b,*]
[a]常州大学石油化工学院先进催化材料与技术重点实验室, 江苏常州213164
[b]清华大学化学系基础分子科学中心, 北京100084

摘要: 水氧化($2H_2O \rightarrow 4e^- + 4H^+ + O_2\uparrow$)是自然以及人工光合作用系统中的关键半反应, 为还原过程提供反应所必需的质子和电子. 但水氧化反应在热力学和动力学上的固有挑战以及对O–O键生成步骤的有限机理认识, 使其成为构筑高效人工光合系统的瓶颈. 为此, 人们开发了大量的金属催化剂, 利用金属中心活化水分子, 并生成活性金属氧物种以促进O–O键的生成. 其间, 金属中心往往需要达到极高的氧化态, 进而导致生成的高价金属氧化物具有极高的催化活性, 极易诱导催化剂降解等副反应的发生, 难以兼顾活性和稳定性. 因此, 深入认识和理解水氧化反应的催化过程及O–O键的生成机制是突破该领域瓶颈的重点. 氧化还原活性配体与金属的协同作用被认为是调节电荷累积过程、平衡催化剂活性与稳定性的有效策略, 受到了广泛的关注. 然而, 氧化还原活性配体调节金属催化中心活性的机理仍有待进一步阐明. 近期, 本研究组发展了一类具有氧化活性配体的单核钌水氧化催化剂$[(L_H^{N5-})Ru^{III}\text{-}OH]^+$, 初步机理研究表明配体的氧化有效地承担了电荷累积, 提出了水分子亲核进攻Ru^{IV}=O形成O–O键的反应机制. 但氧化还原配体的电子效应如何影响催化中心的反应性及其调控规律有待深入研究.

本文设计了一系列具有不同取代基的单核钌催化剂$[(L_R^{N5-})Ru^{III}\text{-}OH]^+$ (R = OMe, **3a**; Me, **3b**; H, **3c**; F, **3d**; CF_3, **3e**), 利用电化学、线性自由能关系以及理论计算等方法考察了配体的电子效应对催化中心活性的调控规律, 并为配体协助下的Ru^{IV}=O催化O–O成键提供了实验证据. 电化学测试结果表明, 在碳酸丙烯酯溶液和0.1 mol/L磷酸缓冲溶液(pH = 7.0)中催化剂均表现出三个连续的氧化峰, 并且配体的取代基效应对其氧化还原电势和催化行为均有显著影响. 但氧化还原电势与取代基常数(σ_{para})的线性相关结果表明, 三个连续的氧化过程表现出了不同的电子效应依赖程度, 第三个氧化过程对电子效应的依赖程度明显高于前两个. 因此三个氧化过程依次被归属为金属中心$Ru^{III/II}$($E(Ru^{III}\text{-}OH/Ru^{II}\text{-}OH_2)$), $Ru^{IV/III}$ ($E(Ru^{IV}=O/Ru^{III}\text{-}OH)$)以及配体中心$L^{+\bullet}/L$ (E $\{[(L^{N5-})^{+\bullet}Ru^{IV}=O]^{2+}/[(L^{N5-})Ru^{IV}=O]^+\}$)的氧化. 催化剂性能测试结果表明, 催化活性和催化过电位均与配体取代基常数(σ_{para})具有良好的线性关系. 随着取代基吸电子能力的增强, 催化剂的转化频率逐渐增大; 随着取代基给电子能力的增加, 催化剂的催化过电位也逐渐降低. 实验结果表明, 氧化还原配体的电子效应可以有效地调控催化剂的催化活性与过电位. 电位与pH相关实验结果表明, 起始的$[(L_R^{N5-})Ru^{III}\text{-}OH]^+$催化剂经历两电子、一质子转移后形成配体氧化的活性中间体$[(L^{N5-})^{+\bullet}Ru^{IV}=O]^{2+}$, 并进一步与水反应生成O–O键. H/D同位素动力学效应及缓冲溶液碱效应证实了水分子亲核进攻$[(L^{N5-})^{+\bullet}Ru^{IV}=O]^{2+}$形成O–O键的机制. 理论计算研究表明, 配体的取代基有效调节了该O–O成键过程的活化能, 进而调控了该决速步的反应速率和催化过电位.

综上, 本文详细阐释了如何通过氧化还原活性配体获得易生成、高活性的金属氧物种, 并调控Ru^{IV}=O中间体对O–O键生成的催化活性, 也为具有低过电位的水氧化催化剂的理性设计和机制研究提供了参考.

关键词: 人工光合作用; 水氧化反应; 氧化还原活性配体; Ru^{IV}=O中间体; 取代基效应

收稿日期: 2023-06-12. 接受日期: 2023-07-28. 上网时间: 2023-09-25.
*通讯联系人. 电子信箱: mtzhang@mail.tsinghua.edu.cn (章名田), zhanght18@tsinghua.org.cn (张洪涛).
基金来源: 国家自然科学基金(21933007, 22193011, 22201024); 江苏省自然科学基金(BK20220617); 江苏省高等学校自然科学基金(21KJB150005); 中国博士后科学基金(2023T160358).